Accepted Manuscript

Hydrogen evolution reaction on bimetallic Ir/Pt(poly) electrodes in alkaline solution

Svetlana Štrbac, Milutin Smiljanić, Thomas Wakelin, Jelena Potočnik, Zlatko Rakočević

PII:	S0013-4686(19)30516-X
DOI:	10.1016/j.electacta.2019.03.100
Reference:	EA 33816
To appear in:	*Electrochimica Acta*
Received Date:	26 October 2018
Accepted Date:	15 March 2019

Please cite this article as: Svetlana Štrbac, Milutin Smiljanić, Thomas Wakelin, Jelena Potočnik, Zlatko Rakočević, Hydrogen evolution reaction on bimetallic Ir/Pt(poly) electrodes in alkaline solution, *Electrochimica Acta* (2019), doi: 10.1016/j.electacta.2019.03.100

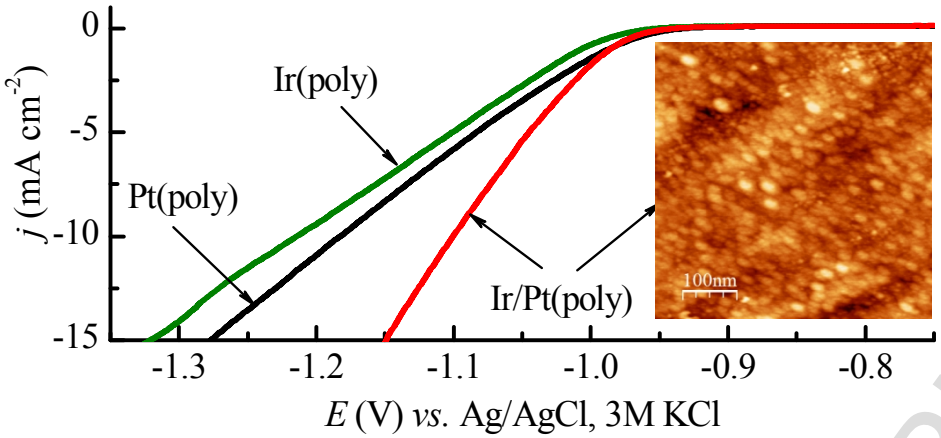

Graphical Abstract

Hydrogen evolution reaction on bimetallic Ir/Pt(poly) electrodes in alkaline solution

Svetlana Štrbac[1]*, Milutin Smiljanić[2], Thomas Wakelin[1†], Jelena Potočnik[2], Zlatko Rakočević[2]

[1]ICTM-Institute of Electrochemistry, University of Belgrade, Njegoševa 12, 11000 Belgrade, Serbia.

[2]INS Vinča, Laboratory of Atomic Physics, University of Belgrade, Mike Alasa 12-14, 11001 Belgrade, Serbia.

Abstract

Hydrogen evolution reaction (HER) was studied in alkaline solution on Pt(poly) electrode modified by spontaneously deposited Ir nanoislands. Comprehensive insight into the characteristics of the bimetallic Ir/Pt(poly) catalysts was obtained by a combination of Atomic Force Microscopy (AFM), Field Emission Scanning Electron Microscopy (FESEM), X-ray Photoelectron Spectroscopy (XPS) and classical electrochemical techniques. HER investigations have shown that the presence of spontaneously deposited Ir enhances the activity of bare Pt(poly) in alkaline solution. This was attributed to the heterogeneity of the active surface sites and to the electronic interaction between two metals in close contact which together facilitated the adsorption of the H intermediate species.

Keywords: platinum; iridium; hydrogen evolution; AFM; FESEM; XPS.

*Author to whom correspondence should be addressed:

E-mail address: sstrbac@tmf.bg.ac.rs

[†]On placement from University of Southampton, Department of Chemistry

1. INTRODUCTION

Depletion of fossil fuel reserves and their ecological footprints are putting the focus on renewable and green energy as one of the current issues of the modern life. Over the last five decades, hydrogen has been considered as the best energy carrier due to its high energy density and zero emission of greenhouse gases [1,2]. Currently, the main obstacle that hinders widespread usage of fuel cells and globalization of the so-called "hydrogen economy" is the fact that hydrogen is still being predominantly produced by the steam reforming of the natural gas and only to a minor extent (~ 4%) from the sustainable processes [3–5]. One of the most convenient routes to obtain green and high purity hydrogen is water electrolysis in which the hydrogen evolution reaction (HER) and the oxygen evolution reaction (OER) occur as the cathodic and anodic processes, respectively [3–6]. Although a major bottleneck for large scale applications of water splitting is sluggish kinetics of OER, a search for advanced cathodic materials for HER is still a hot topic that receives continues attention. Besides being a part of the water splitting and other industrially relevant processes, HER has a pivotal role in the fundamental understanding of electrochemical kinetics and as such is one of the most deeply studied reactions [7,8].

Traditionally, platinum group metals are the most active materials for HER with Pt as the best catalyst that sits on the top of the Volcano plots followed by Rh, Ru and Ir [9–14]. Although the long term idea is to reduce and then to completely replace scarce and expensive metals by more abundant and comparably active materials, Pt-based state of the art catalysts are still the most convenient for the fundamental understanding of the possibilities for the additional optimization of their activities. The main descriptor for the HER activity is the binding energy of the adsorbed H intermediate species, which according to the Sabatier principle should be neither

too strong nor too weak [15]. Therefore, the main route to enhance the activity of Pt is to tune the H binding energy which can be achieved by the modification of Pt catalysts with foreign metals. In this kind of bimetallic structures, electronic properties of Pt can be modulated by the interaction with the foreign metal that affects the H binding energy in a desirable manner and hence promotes HER activity [16]. This would automatically imply that the activities of both constitutive metals for HER are surpassed and that synergism is achieved as the ultimate goal in electrocatalysis. This approach of modifying the Pt catalysts with foreign metal has been widely exploited as a variety of Pt-based binary electrodes have been studied ranging from fundamental works on modified bulk Pt electrodes up to modern Pt based nanoparticles [17–22]. If one focuses on the platinum group metals, representative examples are different Pd-Pt bimetallic structures where presence of Pd promoted the activity of Pt for HER [19,23–26]. In our group, HER was studied on model bimetallic Pd/Pt(poly) electrodes prepared by the spontaneous deposition method which has also shown enhanced activity with respect to bare Pt(poly) [26]. We have extended these studies to the parallel Rh/Pt(poly) system where higher activity for HER than that of Pd/Pt(poly) was observed and explained by the higher susceptibility of the Rh deposit to the electronic interplay with Pt substrate [26].

In a further consideration of feasible model binary electrocatalysts for HER, Ir appears like a good candidate due to its high activity [9–14] and due to the fact that it is already involved in water splitting as one of the most active materials for anodic OER [27,28]. Various Ir-Pt structures were investigated in electrocatalysis of different energy conversion and storage related reactions [29–34], but to the best of our knowledge there are no reports about HER of any kind on bimetallic Ir-Pt catalysts. Concerning the HER, there are several examples where Ir was used to modify Ni-based catalysts and a tendency of approaching the activity of Pt for HER was

observed [35–37]. More recently, our group has shown that Ir/Au(111) structures prepared by the spontaneous deposition exhibited pronounced HER activity in an alkaline solution [38]. These studies showing that Ir can be successfully applied in HER electrocatalysis on model bimetallic electrodes and the mentioned lack of corresponding literature for Ir/Pt structures impose a logical and rather appealing task to investigate HER on bimetallic Ir/Pt catalysts.

In the present contribution, model Ir/Pt(poly) electrodes were prepared via spontaneous deposition as the method commonly used in our group [26]. Bimetallic Ir/Pt(poly) electrodes were characterized by a combination of surface science techniques and classical electrochemical methods. Atomic Force Microscopy (AFM) imaging provided information about surface topography on a nanoscale, and enabled a precise estimation of Ir coverage. Field Emission Scanning Electron Microscopy (FESEM) provided additional characterization of the surface properties on a larger scale and corresponding elemental mapping across Ir/Pt(poly) surface. Insight into the exact chemical nature of spontaneously deposit Ir was obtained by X-ray Photoelectron Spectroscopy (XPS). Cyclic Voltammetry (CV) was explored as a standard electrochemical technique for the characterization of obtained electrodes in alkaline solution. Electrochemical investigations regarding the activity of Ir/Pt(poly) electrodes towards HER were performed in an alkaline solution using Linear Sweep Voltammetry (LSV).

2. EXPERIMENTAL

Pt(poly) rotating disc electrode (5 mm diameter, Pine Instruments Co.) was used as substrate for spontaneous deposition of Ir nanoislands. Electrochemical polishing was applied for preparation and cleaning of the Pt(poly) electrode. Spontaneous deposition was performed by

immersion of Pt(poly) at an open circuit potential (OCP) into 1 mM $IrCl_3 \cdot xH_2O$ solution in 0.05 M H_2SO_4 for the chosen deposition times of 1, 3 and 30 minutes. Extensive rinsing with ultrapure water was applied to prevent the deposition beyond the desired time by removing the excess of Ir solution. After each experiment, Ir deposits were removed by a repetitive electrochemical polishing until a clean Pt(poly) electrode surface was restored. Ir/Pt(poly) electrodes were further subjected to characterization by a combination of surface science techniques.

AFM was used to reveal nanoscale surface properties of bimetallic Ir/Pt(poly) electrodes. *Ex situ* AFM imaging was performed under ambient conditions in the tapping mode using MultiMode Quadrex SPM with Nanoscope IIIe controller (Veeco Instruments, Inc). Surface features of Ir/Pt(poly) catalysts such as morphology, size, distribution of Ir nanoislands and total Ir coverage were obtained by simultaneous recording of height and phase AFM images across various sites over the electrode surface.

Field Emission Scanning Electron Microscopy with Energy Dispersive X-ray Spectrometer, (FESEM-EDS, FEI Scios 2) was used for morphology studies, as well as for elemental composition studies of the Ir/Pt(poly) catalyst. The acceleration voltage between cathode and anode was equal to 12 kV. A freshly prepared sample was analyzed by FESEM and EDS at the pressure of 8.2 × 10-5 Pa.

XPS was used to get an insight into the surface chemical composition and into the electronic state of the surface constituents of bare Pt(poly) and Ir/Pt(poly) electrode obtained for 30 min deposition. SPECS System with XP50M X-ray source for Focus 500 and PHOIBOS 100/150 analyzer, and AlKα source (1486.74 eV) at a 12.5 kV and 32 mA was used for this study. XPS spectra were obtained at a pressure in the range of 3×10^{-8} - 2×10^{-9} mbar. Survey X-

ray photoelectron spectra of both electrodes were recorded first in the binding energy region from 0-1000 eV, with the energy step of 0.2 eV, dwell time 0.5 s and pass energy of 40 eV in the FAT mode. From these spectra the binding energy regions of the main peaks of the elements from which the corresponding electrodes were composed of were identified. The C 1s photoelectron line originating from carbon as a contaminant was also identified in both cases at the same position of 283.7 eV. Accordingly, high resolution spectra of the main 4f peaks characteristic for Pt and Ir, as well as O 1s and Cl 2p peaks were recorded with the energy step of 0.1 eV. Due to the low intensity, the XPS data for Ir 4f peaks were obtained as a sum of 10 consecutive scans. The XPS data were collected by SpecsLab data analysis software and analyzed using CasaXPS software, both provided by the manufacturer.

Electrochemical measurements were performed in a conventional three electrode cell, with Pt(poly) (bare or modified) as the working electrode, Pt wire as the counter electrode and Ag/AgCl, 3 M KCl as the reference electrode. All potentials in this work are quoted with respect to the used reference electrode. Electrochemical characterization of bare Pt and Ir/Pt(poly) electrodes was conducted by cyclic voltammetry in 0.1 M NaOH solution at a scan rate of 50 mV s^{-1}. Activities of modified electrodes for HER were investigated by linear sweep voltammetry in the same alkaline electrolyte saturated with molecular hydrogen at a scan rate of 10 mV s^{-1}.

Steady-state measurements were performed for Pt(poly), Ir(poly) and the most active 1 min Ir/Pt(poly) electrodes in hydrogen saturated electrolyte in order to obtain Tafel plots for a proper evaluation of a Tafel slope as a crucial parameter in HER mechanism. Starting from the value sufficiently more positive than the theoretical equilibrium potential for HER (-0.98 V *vs.* Ag/AgCl, 3M KCl reference electrode in 0.1 M NaOH), the applied electrode potential was decreased sequentially until equilibrium HER potential of -0.967 V, at which current equals zero,

was determined. Slight deviation (~13 mV) from the theoretical value can be linked with the deviation of the potential of the used reference electrode from the ideal value. The overpotential for HER is then calculated as the difference between determined equilibrium potential and the measured potential. Chronoamperometric curves were recorded up to the overpotential of 120 mV with the step of 5 mV. Each applied potential was held for 200 s and a corresponding chronoamperometric response was recorded. Rotation of the electrodes at 1600 rpm was applied to prevent the accumulation of the evolved hydrogen. Steady-state current density values were taken for t = 200 s (usually established already at t ≤ 100 s) for Tafel slopes construction.

It is important to note that all electrochemical measurements were conducted in entirely separated experimental setups starting from electrode cleaning and preparation. This ensures controlled reproducibility and prevents any artifacts related to the changes in the structure of modified electrodes due to the previous experimental work. Before each electrochemical experiment, bimetallic electrodes were held at the potential of -0.45 V during 15 minutes in the nitrogen saturated 0.1 M NaOH electrolyte to promote stabilization of Ir deposit.

Since all electrochemical measurements have been performed in alkaline electrolyte, glass corrosion and subsequently its influence on the catalytic activity of examined electrodes for HER should be taken into account according to previous reports [39,40]. However, we believe that glass corrosion does not play a decisive role in this work due to the several experimental conditions. Namely, 0.1 M NaOH electrolyte was prepared daily fresh in the thoroughly cleaned glass volumetric flask and it was consumed briefly (t < 2h). Collecting of the CV or LSV curves usually lasted less than 30 minutes and then cell was disassembled and thoroughly cleaned for the next measurement. When using bare Pt as working electrode even for a longer time than given above, we have not observed the pronounced influence of the glass corrosion on the CV

features as seen in refs. [39,40]. Therefore, in the cases of recording of the CVs and LSV curves the leaching of the glass from both volumetric flask and cell due to the contact with alkaline solution should be minimized. However, the current drop observed during steady state measurements can be associated with the glass corrosion since these experiments demanded more time.

Depositing solution was prepared from $IrCl_3 \cdot xH_2O$ and suprapure H_2SO_4 manufactured by Mateck and Merck, respectively. Working electrolyte solutions were prepared from NaOH pellets provided by Merck and deaerated by purging with high purity nitrogen (99.999%, Messer) for at least 15 minutes, or saturated by bubbling the high purity hydrogen (99.999%, Messer) during 10 minutes. All solutions were diluted with ultrapure water (Milli-Q from Millipore). All experiments were performed at room temperature.

3. RESULTS AND DISCUSSION

3.1. Spontaneous deposition of Ir on Pt(poly)

Spontaneous deposition was carried out by immersion of Pt(poly) substrate into 1 mM $IrCl_3$ + 0.05 M H_2SO_4 solution at open circuit potential (OCP). Monitoring of the OCP during the spontaneous deposition can provide insight into the deposition rate and possible oxidation states of the deposit and the substrate. For these purposes, chronopotentiometric curves recorded during 30 minutes of immersion of Pt(poly) into Ir containing and Ir free 0.05 M H_2SO_4 solution and during the contact of Ir(poly) electrode 0.05 M H_2SO_4 free of Ir ions, and corresponding cyclic voltammograms are presented in Fig. 1.

Spontaneous deposition rate can be discussed through the change of the OCP with time, Fig. 1a. For both bare Pt(poly) and Ir(poly) immersed into the base 0.05 H_2SO_4 solution, the OCP decreases upon immersion due to the specific adsorption of sulfate anions and reaches a plateau after a certain immersion time when the adsorption/desorption equilibrium is established. When Pt(poly) electrode is immersed into the same base solution containing Ir depositing anions, the OCP value decreases during the first couple of minutes. With the prolongation of time (t > ~4 min), OCP changes are far less pronounced meaning that deposition slows down. This could indicate that saturation coverage of Ir is reached within first several minutes of deposition and that it does not change significantly with further prolongation of the time. It should be noted that the initial decay of the OCP is associated to the specific adsorption of both sulfate anions from the base solution and negatively charged Ir complexes (see ref. [38]), resulting in the formation of Ir deposit, the nature of which will be determined by XPS.

CV curves of bare Pt, Ir and 30 min Ir/Pt electrodes recorded in 0.05 M H_2SO_4 solution free of Ir ions are presented in Fig. 1b. Since CV characterization of all electrodes was performed in alkaline solution and will be discussed later on, CVs in acid solution will not be discussed in details. CVs of Pt(poly) [41] and Ir(poly) [42] electrodes are in good agreement with literature data, while CV of 30 min Ir/Pt(poly) electrode shows clear changes with respect to the Pt(poly) as the first confirmation of the presence of spontaneously deposited Ir. These changes are primarily referred to the suppression of H_{upd} and Pt oxide formation/reduction peaks. The values of the OCP established during Ir deposition on Pt (Fig. 1a) are matching with the oxidation region of Pt(poly), Ir(poly) and Ir/Pt(poly) electrodes (Fig. 1b). This indicates that Ir is at least partly deposited in its oxide form on top of Pt(poly) substrate, which can also be partly oxidized.

Additionally, thermodynamic possibility of spontaneous deposition of Ir on Pt requires comparison of the standard half reaction potentials corresponding to the oxidation of Pt substrate and reduction of Ir species from the depositing solution. Acid solution of $IrCl_3xH_2O$ used in this work contains a mixture of Ir^{3+} and Ir^{4+} complexes in the redox equilibrium as already summarized in ref. [38]. Namely, species like $Ir(H_2O)_3Cl_3$ and $[Ir(OH)_6]^{3-}$, $[IrCl_6]^{3-}$, $[IrCl_6]^{2-}$ and $[Ir(OH)_6]^{2-}$ can be present depending on the aging of the solution. This means that during Ir deposition on Pt(poly) substrate Ir^{3+}/Ir^{4+} species would be reduced while Pt substrate would be oxidized (electroless deposition). Since thermodynamically this process would not occur spontaneously, this means that in this case some other mechanism should be taken into consideration. This will be further corroborated by the analyses of the exact chemical composition of the Ir/Pt(poly) electrode, using XPS as will be shown below.

3.2. AFM surface topography and phase imaging

AFM height image of bare Pt(poly) substrate surface is presented in Fig. 2. Topography of polycrystalline platinum is shown in Fig. 2a, where it can be seen that the surface consists of smaller domains of various facets. Cross section along the line indicated in the image, Figure 2b, shows that these facets are approximately 20 to 50 nm wide and up to 6 nm high. The phase image is not shown as there is no deposit on the surface, meaning that there is no chemical contrast to be observed.

Height and phase AFM images of Ir/Pt(poly) obtained after 1 min deposition have already been reported in ref. [43]. The coverage of Pt(poly) substrate with the deposited Ir islands was (80 ± 2)%. The individual Ir islands, 10 – 25 nm wide, and 0.25 – 1 nm high, were agglomerated to form larger (up to 100 nm) islands. AFM images of the Ir/Pt(poly) electrode

obtained after 30 minute Ir deposition are shown in Fig. 3. The surface topography giving the height and width of the deposited Ir islands is given in Fig. 3a. The cross section outlined by the line on Fig. 3a, giving the heights and widths of the deposited islands is presented in Fig. 3b. The red dotted line on Fig. 3b indicates where the bulk platinum surface ends and the iridium islands starts. The height of the islands ranged from around 0.25 – 1.5 nm or around 1 – 4 monolayers. Furthermore the image also shows that the width of the islands range from 50 – 150 nm. The variations of the chemical composition of the Ir/Pt(poly) surface are shown by corresponding phase AFM image given in Fig. 3c. The difference in chemical composition across the line on Fig. 3c is shown in Fig. 3d. The blue dashed line on Fig. 3d divides the exposed platinum surface below and above the line the deposited iridium. From this image we take the threshold for bare Pt to be at – 3.0°. This limit is then used to produce Fig. 3e where the blue color (background color) represents the bare Pt surface and the yellow the deposited Ir. From Fig. 3e, coverage of (95 ± 2)% for the 30 minute deposited iridium on Pt(poly) was estimated. In Fig. 3f one can see the width of the islands from a cross section on Fig. 3e, represented by the line, where in this case the islands range from 50 – 100 nm.

3.3. FESEM-EDS characterization

FESEM analysis of the bi-metallic Ir/Pt(poly) electrode and its corresponding EDS elemental mapping are shown in Fig. 4. The FESEM micrograph of the analyzed sample is presented in the Fig. 4a. EDS elemental mapping of deposited Ir onto Pt(poly) is given in Fig. 4 (b - d). In addition to the deposited Ir, the presence of oxygen on the sample surface is also noticed. Oxygen, iridium and platinum are presented with different colors: O (grey), Ir (cyan)

and Pt (yellow). The images show that oxygen is present in traces on the sample surface, while iridium is distributed relatively uniformly over the specimen.

A typical X-ray spectrum, collected with an EDS system from the area observed in Fig. 4a is shown in Fig. 4e. The EDS spectrum directly revealed the presence of the atomic elements O, Ir and Pt on the sample surface. These peaks occur in the energy range of 0.2 keV to approximately 4 keV. It can be seen from the spectrum that the peaks for Pt and Ir are overlapped. Since Pt and Ir have very similar atomic weights, EDS mapping was not able to easily distinguish these two peaks. Similar overlapping of Ir and Pt peaks was found for IrPt alloy nanoparticles designed for electrocatalytic applications [44].

3.4. XPS spectra of Ir/Pt(poly))surface

High resolution spectra of Pt 4f doublets for bare Pt(poly) and for Ir/Pt(poly) electrodes are presented in Fig. 5. For both electrodes, Pt 4f doublets are fitted to two components. For bare Pt(poly), Fig. 5a, the first component, which consists of $4f_{7/2}$ and $4f_{5/2}$ lines positioned at 70.4 eV and 73.7 eV, respectively, correspond to metallic platinum [45,46]. The second component consisting of $4f_{7/2}$ and $4f_{5/2}$ lines positioned at 71.9 eV and 75.2 eV, respectively, correspond to PtO [46]. The peak separation of 3.3 eV in both cases is in agreement with literature data [45,46]. When Pt(poly) surface is covered with Ir overlayer, Fig. 5b, the positions of both lines corresponding to metallic Pt remain unchanged, while the ones corresponding to PtO are shifted to lower binding energies: $4f_{7/2}$ for 0.2 eV and $4f_{5/2}$ for 0.4 eV. Consequently for the latter one the peak separation changes to 3.1 eV. This down shift of Pt 4f binding energies infers to the electronic effect caused by the presence of the deposited Ir overlayer.

High resolution spectra of Ir 4f, O 1s and 2p photoelectron lines for Ir/Pt(poly) are presented in Fig. 6. Both Ir $4f_{7/2}$ and $4f_{5/2}$ lines are fitted to two components, Fig. 6a. The first component at lower binding energies consists of two peaks at 61.1 eV and 63.9 eV, which according to the literature data (60.8 eV and 63.8 eV in ref. [47]) correspond to metallic iridium. The second doublet at higher binding energies of 61.8 eV and 64.6 eV correspond to either IrO_2 (61.9 eV and 64.9 eV in ref. [47]) or to $Ir(OH)_3$ (62.0 eV and 65.0 eV in ref. [48]). In both cases Ir doublets separation is 2.8 eV, a bit lower than 3.0 eV according to literature data [47].

O 1s photoelectron line is fitted to two components, Fig. 6b. The first component at lower binding energy of 530.8 eV can be ascribed to originate from either IrO_2 (530.5 eV in ref. [47]) or from PtO (530.5 eV in ref. [48]). Besides, O 1s line recorded together with spectra for bare Pt(poly) from Fig. 5a, is positioned at 531.0 eV (not presented) and its origin can be ascribed to PtO. The second component, at higher binding energy of 532.2 eV can be assigned to hydroxide species (531.5 eV in ref. [47], and 532.0 eV in ref. [48]). This analysis of O 1s binding energies confirms the presence of both IrO_2 and $Ir(OH)_3$.

Cl 2p photoelectron line is fitted to two components, Fig. 6c. Cl 2p doublet consists of two lines, $2p_{3/2}$ at 198.4 eV and $2p_{1/2}$ at 200.0 eV, with the proper doublet separation of 1.6 eV. According to literature, this chlorine originates from solvated hydrochloric acid, $HCl{\cdot}nH_2O$ (198.3 eV in ref. [49]). It is worth noting that there are no Cl 2p lines which can be associated with chlorine originating from any IrClx species (Cl $2p_{3/2}$ at 199.2 eV in ref. [50]), confirming the analysis above according to which Ir is spontaneously deposited on Pt as a mixture of metallic Ir and IrOx species. In contrast to this case, when Ir is spontaneously deposited from the same solution on Au as substrate, the deposit consists of $IrCl_3$ and IrOx, but no metallic Ir [38]. The Cl 2p peak at 197.0 eV can be assigned to chloride originating from HCl chemisorbed not

directly at Ir metal site but on preoxidized Ir like in the case of Pd, where it undergoes chemisorbed replacement reaction [51].

To summarize, XPS analysis of bimetallic Ir/Pt(poly) surface has revealed that Ir is spontaneously deposited as a mixture of metallic Ir, IrO_2 and $Ir(OH)_3$ species. Since XPS measurements were performed immediately after the spontaneous deposition and electrode rinsing with water, we believe that the composition of the surface should not change during the brief electrode transfer into XPS chamber. For the electrochemical measurements (see below), the bimetallic electrodes were additionally protected by a droplet of water during the transfer into the cell, thus their exposure to the ambient conditions is minimized again. However, it can be assumed that the relative amount of metallic Ir and Ir-oxide species changes during the exposure of the bimetallic electrode to the alkaline solution and potential applied during electrochemical measurements.

According to these XPS results, we can now propose that spontaneous deposition of Ir on Pt(poly) involves the adsorption and the discharge of different Ir^{3+}/Ir^{4+} complexes, which are further decomposed and oxidized on the surface of Pt. Similarly as in the case of Rh/Au(111) [52], Pt substrate most likely acts only as a catalysts for spontaneous deposition, but not as a reducing agent. Since spontaneous deposition of Ir on Pt(poly) was performed from non-deaerated depositing solution, we assume that the OCP presents a mixed potential between cathodic oxygen reduction reaction and a partial anodic oxidation of Pt and Ir. In the case when Pt electrode is immersed into the base solution containing Ir depositing anions, the discharge of the adsorbed Ir complexes takes part as the anodic reaction similarly like in the case of Rh/Au(111) system [52].

3.5. Electrochemical characterization of Ir/Pt(poly) electrodes

Electrochemical characterization of Ir/Pt(poly) electrodes was carried out in 0.1 M NaOH and the obtained CVs are given in Fig. 7. For adequate comparison, Fig. 7 is supplemented with the CV profiles of bare Pt(poly) and Ir(poly) electrodes. Potential window for Pt(poly) and Ir/Pt(poly) electrodes was set between -0.85 V and -0.45 V, while for Ir(poly) negative potential limit was extended to -0.90 V in order to include full H_{upd} region. Current densities are referred to electrochemically active surface areas (EASAs) calculated from the CO stripping voltammetry, as shown in our recent work [43]. EASA values were 0.21 cm^2, 0.25 cm^2, 0.22 cm^2, 0.23 cm^2 and 0.23 cm^2 for Pt(poly), Ir(poly), 1 min Ir/Pt(poly), 3 min Ir/Pt(poly) and 30 min Ir/Pt(poly) electrodes, respectively.

In accordance with previous reports, CV profile of bare Pt(poly) contains two pairs of reversible H_{upd} peaks placed at the potentials of -0.69 V and -0.57 V [26,53]. As for Ir(poly), three pairs of reversible peaks centered at -0.82 V, -0.73 V and -0.64 V appear in H_{upd} region, which is again in good agreement with literature [54,55].

The main features of the CVs corresponding to the Ir/Pt(poly) electrodes are the potential shifts of the H_{upd} peaks and the suppression of their intensities with respect to the bare Pt(poly). The first H_{upd} peak is broadened and shifted to the more negative potentials on which H_{upd} does not occur on bare Pt but it occurs on Ir. The second H_{upd} peak is barely distinguishable and also shifted negatively with respect to the bare Pt(poly). This clearly indicates that the energetics of the interaction of the bimetallic surfaces with the adsorbed H_{upd} species is changed with respect to the bare Pt(poly). The suppression of the H_{upd} peaks becomes more pronounced as the Ir coverage increases which indicates increasing inaccessibility of the Pt surface for the adsorption of H_{upd} species. The explanation for the suppression of the H_{upd} peaks can be found in the

presence of non-metallic Ir species on top of Pt(poly), similarly like in the case of Ir/Au(111) electrodes [38]. This assumption is in line with the discussion about the XPS spectra of Ir/Pt(poly) electrode (see Fig. 6) according to which the presence of oxide Ir species is detected. The fact that spontaneously deposited Ir-oxide species are not completely reduced after recording of the cyclic voltammograms in the given potential limits preceded by the potential holding also indicate the presence of non-reducible IrOx as suggested earlier in ref. [38]. As a consequence of the suppression of H_{upd} peaks EASA cannot be calculated from the charge under the H_{upd} peaks, which is otherwise used for EASA determination of both bare Pt(poly) and Ir(poly) [56]. In contrast to this, CO stripping voltammetry, as another commonly used method for EASA evaluation [56], showed slight increase of the EASAs for the bimetallic Ir/Pt(poly) electrodes with respect to Pt(poly) [43].

3.6. HER on bimetallic Ir/Pt(poly) electrodes in alkaline solution

The activities of bimetallic Ir/Pt(poly) electrodes for HER were investigated in hydrogen saturated 0.1 M NaOH solution by LSV. Collected polarization curves together with the ones corresponding to the bare Pt and Ir electrodes are given in Fig. 8. It is clear that the order of activities for HER follows the line Ir(poly) < Pt(poly) < Ir/Pt(poly), meaning that synergism is achieved for bimetallic electrodes. Pt(poly) and Ir/Pt(poly) electrodes exhibit similar activities at the onset of the hydrogen evolution reaction, while bimetallic electrodes become more active with the increase of the overpotential. Among different Ir/Pt(poly) electrodes, the one obtained for 1 min Ir deposition (with the lowest Ir coverage of 80%) has shown the highest activity, which decays with the increase of the Ir coverage. Potential corresponding to the current density of -10 mA cm^{-2} shows the enhancement of 80 mV for 1 min Ir/Pt(poly) electrode with respect to

Pt(poly), which drops down to around 50 and 20 mV for Ir/Pt(poly) electrodes obtained after 3 and 30 minutes of deposition, respectively.

Tafel plots constructed using the data from steady–state measurements of HER on Ir(poly), Pt(poly) and 80% Ir/Pt(poly) in hydrogen saturated 0.1 M NaOH are given in Fig. 9. As an illustration a set of chronoamperometry curves recorded at η = 50 mV is given as an inset. Tafel analysis demand a brief recalling of the HER mechanism. In alkaline media hydrogen evolution reaction begins with the adsorption of H intermediate through the discharge of water in the so-called Volmer step. In the next step, H intermediate species ought to be removed from the catalyst surface to enable further continuation of the reaction. This can be achieved either through the chemical recombination of two adsorbed H intermediates in the so-called Tafel step or through the electrochemical recombination in the so-called Heyrovsky step [57,58].

For all examined electrodes, Tafel slopes of -(60 ± 5) mV dec^{-1} and -(120 ± 5) mV dec^{-1} were fitted at lower and higher overpotentials, respectively. The obtained values and the change of the Tafel slopes with the increase of the overpotential are in accordance with earlier studies of HER on different Pt electrodes in alkaline solutions [59,60]. Mechanism of HER appears to follow both Volmer-Tafel and Volmer-Heyrovsky pathways, the former being predominant at low overpotentials, while the latter prevails with the increase of the overpotential [26,59,60]. However, there are studies of HER kinetics on Pt in alkaline media that showed only one defined Tafel slope of -120 mV dec^{-1} which is ascribed to the Volmer-Heyrovsky mechanism [61,62]. Since DFT calculations have shown that the activation energies for both Tafel and Heyrovsky steps on Pt are comparable [63], and taking into account our observations, we find it reasonable to assume that both mechanisms are operative but at different overpotentials.

The origin of the enhanced catalytic activity of Ir/Pt(poly) electrodes for HER can be found in tuning of the H intermediate binding strength through the electronic interaction between Pt substrate and Ir deposit. The highest HER activity is obtained for 80% Ir/Pt(poly) electrode (the lowest coverage among investigated electrodes), which can be related with the most pronounced surface heterogeneity. It can be supposed that bimetallic surface heterogeneity involving bare Pt sites, Ir islands and bimetallic Ir/Pt junctions on this particular 80% Ir/Pt(poly) surface causes the strongest electronic interplay between Pt substrate and Ir deposit. Accordingly, HER commences by the adsorption of H intermediate on Ir/Pt junctions as energetically the most favorable sites and proceeds further on the other active sites as well. With the increase of Ir coverage up to the full, the Ir islands height also increases, while the heterogeneity of the surface decreases. Consequently, the electronic interplay between the underlying Pt and the deposited Ir islands weakens. This leads to the slight decrease of the HER activity, although it still remains higher than the activity of bare Pt(poly) electrode.

Additionally, it is interesting to compare hereby presented results with our earlier report concerning HER on parallel Pd/Pt(poly) and Rh/Pt(poly) electrodes [26]. While the coverage of the most active Ir/Pt(poly) and Rh/Pt(poly) electrodes were comparable (80% Ir *vs.* 75% Rh), the coverage of Pd in the most active Pd/Pt(poly) was 50%. All these bimetallic electrodes are more active for HER than bare Pt(poly) with the order of activities Rh/Pt(poly) > Pd/Pt(poly) > Ir/Pt(poly), and in all cases explanation of the enhancement was in the electronic interaction between the deposit and Pt substrate. Besides the sole nature of the deposited metals, observed trend in the activities can be explained by taking into account the influence of the deposit structure on the electronic interaction with Pt substrate. The order of activities between Rh/Pt(poly) and Pd/Pt(poly) electrodes was explained by the difference in the structures of the

deposits, as Rh islands were smaller in size and homogeneously distributed, while Pd islands were larger, agglomerated and randomly distributed. This led to the more pronounced electronic interaction in the case of Rh/Pt(poly) electrodes and hence to the higher activity for HER. In the case of Ir/Pt(poly), the Ir islands are also agglomerated into larger and wider domains which can lead to the less pronounced electronic interplay with Pt substrate than in the cases of both Rh and Pd. As a consequence, catalytic effect of spontaneously deposited Ir on the activity of Pt(poly) for HER is slightly lower than in the cases of Pd and Rh. Nevertheless, the synergistic effect observed for model Ir/Pt(poly) electrodes certainly opens up an outlook towards bimetallic Ir-Pt nanostructures as feasible catalysts for HER.

4. CONCLUSION

In this work, we have demonstrated that the presence of spontaneously deposited Ir enhances the activity of Pt(poly) for hydrogen evolution in alkaline solution. AFM imaging has revealed that Ir coverage ranged from 80% up to a full coverage depending on the applied deposition time. Elemental mapping of the Ir/Pt(poly) electrode, provided by FESEM-EDS, has detected the presence of Ir, which was further shown to be spontaneously deposited as a mixture of metallic Ir and IrOx species by a corresponding XPS analysis. HER investigations revealed that all Ir/Pt(poly) electrodes were more active than bare Pt(poly), meaning that synergistic effect was achieved. 80% Ir/Pt(poly) exhibited the highest activity, which slightly decayed at higher Ir coverage but still remained more active than Pt substrate. The enhancement of the HER activity and the observed inverse correlation between the activities of Ir/Pt(poly) electrodes and increasing Ir coverage were ascribed to the suitable alteration of the binding energy of H

intermediate adsorption as the first step in HER mechanism. Both the heterogeneity of the active surface sites and the electronic interaction between Pt substrate and Ir deposit are the main factors contributing to the observed synergistic effect.

Acknowledgement: The work was supported by the Ministry of Education, Science and Technological Development, Republic of Serbia, project N^{o} 45005.

References

1. M. Momirlan, T.N.Veziroglu, The properties of hydrogen as fuel tomorrow in sustainable energy system for a cleaner planet, *Int. J. Hydrogen Energy* 30 (2005) 795–802.
2. M. Ball, M. Weeda, The hydrogen economy - Vision or reality? *Int. J. Hydrogen Energy* 40 (2015) 7903–7919.
3. R.F. de Souza, J.C. Padilha, R.S. Goncalves, M.O. de Souza, J. Rault-Berthelot, Electrochemical hydrogen production from water electrolysis using ionic liquid as electrolytes: Towards the best device*, J. Power Sources* 164 (2007) 792–798.
4. D.M.F. Santos, C.A.C. Sequeira, J.L. Figuereido, Hydrogen production by alkaline water electrolysis, *Quim. Nova* 36 (2013) 1176–1193.
5. G.W. Crabtree, M.S. Dresselhaus, M.V. Buchanan, The hydrogen economy, *Phys. Today* 57 (2004) 39–44.
6. I. Vincent, D. Bessarabov, Low cost hydrogen production by anion exchange membrane electrolysis: A review, *Renew. Sust. Energ. Rev.* 81 (2018) 1690–1704.
7. D. Strmčnik, P.P. Lopes, B. Genorio, V.R. Stamenković, N.M. Marković, Design principles for hydrogen evolution reaction catalyst materials, *Nano Energy* 29 (2016) 29–36.
8. A. Eftekhari, Electrocatalysts for hydrogen evolution reaction, *Int. J. Hydrogen Energy* 42 (2017) 11053–11077.
9. S. Trasatti, Work function, electronegativity and electrochemical behaviour of metals: electrolytic hydrogen evolution in acid solutions, J. *Electroanal. Chem.* 39 (1972) 163–182.

10. W. Sheng, M. Myint, J.G. Chen, Y. Yan, Correlating the hydrogen evolution reaction activity in alkaline electrolytes with the hydrogen binding energy on monometallic surfaces, *Energy Environ. Sci*. 6 (2013) 1509–1512.
11. P. Quaino, F. Juarez, E. Santos, W. Schmickler, Volcano plots in hydrogen electrocatalysis – uses and abuses, *Beilstein J. Nanotechnol.* 5 (2014) 846–854.
12. J.K. Nørskov, T. Bligaard, A. Logadottir, J.R. Kitchin, J.G. Chen, S. Pandelov, U. Stimming, Trends in the exchange current for hydrogen evolution, *J. Electrochem. Soc.* 152 (2005) J23–J26.
13. J. Greeley, T.F. Jaramillo, J. Bonde, I. Chorkendorff, J.K. Norskov, Computational high-throughput screening of electrocatalytic materials for hydrogen evolution, *Nat. Mater.* 5 (2006) 909–913.
14. A. Lasia, Hydrogen evolution reaction, in: W. Vielstich, A. Lamm, H.A. Gasteiger (Eds.), *Handbook of Fuel Cells – Fundamentals, Technology and Applications,* Vol. 2, Ch. 4.6, J. Wiley & Sons, Ltd, Chichester, 2003, 414–460.
15. P. Sabatier, Hydrogenations et deshydrogenations par catalyse, *Ber. Deut. Chem. Gesell.* 44 (1911) 1984–2001.
16. J. Tymoczko, F. Calle-Vallejo, W. Schuhmann, A.S. Bandarenka, Making the hydrogen evolution reaction in polymer electrolyte membrane electrolysers even faster, *Nat. Commun.* 7 (2016) N^0 10990.
17. W. Yu, M.D. Porosoff, J.G. Chen, Review of Pt-based bimetallic catalysis: From model surfaces to supported catalysts, *Chem. Rev.* 112 (2012) 5780–5817.

18. W. Wu, Z. Tang, K. Wang, Z. Liu, L. Li, S. Chen, Peptide templated AuPt alloyed nanoparticles as highly efficient bi-functional electrocatalysts for both oxygen reduction reaction and hydrogen evolution reaction, *Electrochim. Acta* 260 (2018) 168–176.
19. N.M. Marković, C.A. Lucas, V. Climent, V. Stamenković, P.N. Ross, Surface electrochemistry on an epitaxial palladium film on Pt(111): surface microstructure and hydrogen electrode kinetics, *Surf. Sci.* 465 (2000) 103–114.
20. W. Shen, B. Wu, F. Liao, B. Jiang, M. Shao, Optimizing the hydrogen evolution reaction by shrinking Pt amount in Pt-Ag/SiNW nanocomposites, *Int. J. Hydrogen Energy* 42 (2017) 15024–15030.
21. M.A. Dominguez-Crespo, E. Ramirez-Meneses, A.M. Torres-Huerta, V. Garibay-Febles, K. Philippot, Kinetics of hydrogen evolution reaction on stabilized Ni, Pt and Ni-Pt nanoparticles obtained by an organometallic approach, *Int. J. Hydrogen Energy* 37 (2012) 4797–4811.
22. X. Weng, Y. Liu, K.K. Wang, J.J. Feng, J. Yuan, A.J. Wang, Q.Q. Xu, Single-step aqueous synthesis of AuPt alloy nanodendrites with superior electrocatalytic activity for oxygen reduction and hydrogen evolution reaction, *Int. J. Hydrogen Energy* 41 (2016) 18193–18202.
23. R. Ojani, J.B. Raoof, E. Hasheminejad, One-step electroless deposition of Pd/Pt bimetallic microstructures by galvanic replacement on copper substrate and investigation of its performance for the hydrogen evolution reaction, *Int. J. Hydrogen Energy* 38 (2013) 92–99.
24. M. Wu, P.K. Shen, Z. Wei, S. Song, M. Nie, High activity PtPd-WC/C electrocatalyst for hydrogen evolution reaction, *J. Power Sources* 166 (2007) 310–316.

25. B. Rezaei, M. Mokhtarianpour, A.A. Ensafi, Fabrication of bimetallic Pd/Pt nanostructure deposited on copper nanofoam substrate by galvanic replacement as an effective electrocatalyst for hydrogen evolution reaction, *Int. J. Hydrogen Energy* 40 (2015) 6754–6762.
26. M. Smiljanić, Z. Rakočević, A. Maksić, S. Štrbac, Hydrogen evolution reaction on platinum catalyzed by palladium and rhodium nanoislands, *Electrochim. Acta* 117 (2014) 336–343.
27. T. Reier, D. Teschner, T. Lunkenbein, A. Bergmann, S. Selve, R. Kraehnert, R. Schlogl, P. Strasser, Electrocatalytic oxygen evolution on iridium oxide: uncovering catalyst-substrate interactions and active iridium oxide species, *J. Electrochem. Soc.* 161 (2014) F867–F882.
28. T. Reier, M. Oezaslan, P. Strasser, Electrocatalytic oxygen evolution reaction (OER) on Ru, Ir, and Pt catalysts: A comparative study of nanoparticles and bulk materials, *ACS Catal.* 2 (2012) 1765–1772.
29. E.N. El-Sawy, H.M. Molero, V.I. Birss, Methanol oxidation at porous co-electrodeposited Pt-Ir thin films, *Electrochim. Acta* 117 (2014) 202–210.
30. E.I. Papaioannou, A. Siokou, Ch. Comninellis, A. Katsaounis, Pt–Ir Binary Electrodes for Direct Oxidation of Methanol in Low-Temperature Fuel Cells (DMFCs), *Electrocatal.* 4 (2013) 375–381.
31. M. Wesselmark, B. Wickman, C. Lagergren, G. Lindbergh, The impact of iridium on the stability of platinum on carbon thin-film model electrodes, *Electrochim. Acta* 111 (2013) 152–159.

32. B. Wu, J. Zhu, X. Li, T. Zhou, L. Mao, S. Xiong, Electrodeposition of platinum-iridium nanoparticles on carbon nanotubes and their electrocatalytic oxidation of glucose, *Indian J. Chem. Sec. A* 56A (2017) 1007–1013.

33. S.H. Chang, M.H. Yeh, J. Rick, W.N. Su, D.G. Liu, J.F. Lee, C.C. Liu, B.J. Hwang, Bimetallic catalyst of PtIr nanoparticles with high electrocatalytic ability for hydrogen peroxide oxidation, *Sens. Actuators. B Chem.* 190 (2014) 55–60.

34. W. Chen, S. Chen, Iridium-platinum alloy nanoparticles: Composition-dependent electrocatalytic activity for formic acid oxidation, *J. Mater. Chem.* 21 (2011) 9169–9178.

35. M. Duca, E. Guerrini, A. Colombo, S. Trasatti, Activation of nickel for hydrogen evolution by spontaneous deposition of iridium, *Electrocatal.* 4 (2013) 338–345.

36. K.A. Kuttiyiel, K. Sasaki, W.F. Chen, D. Su, R.R. Adžić, Core-shell, hollow-structured iridium-nickel nitride nanoparticles for the hydrogen evolution reaction, *J. Mater. Chem. A* 2 (2014) 591–594.

37. A. Papaderakis, N. Pliatsikas, P. Patsalas, D. Tsiplakides, S. Balomenou, A. Touni, S. Sotiropoulos, Hydrogen evolution at Ir-Ni bimetallic deposits prepared by galvanic replacement, *J. Electroanal. Chem.* 808 (2018) 21–27.

38. S. Štrbac, I. Srejić, Z. Rakočević, Electrocatalysis of hydrogen evolution reaction on Au(111) by spontaneously deposited iridium in acid solution, *J. Electrochem. Soc.* 165 (2018) J3335–J3341.

39. K.J.J. Mayrhofer, G.H.K. Wiberg, M. Arenz, Impact of glass corrosion on the electrocatalysis on Pt electrodes in alkaline electrolyte, *J. Electrochem. Soc.* 155 (2008) P1–P5.

40. K.J.J. Mayrhofer, A.S. Crampton, G.H.K. Wiberg, M. Arenz, Analysis of the impact of individual glass constituents on electrocatalysis on Pt electrodes in alkaline solution, *J. Electrochem. Soc.* 155 (2008) P78–P81.

41. D.A.J. Rand, R. Woods, A study of the dissoulution of the platinum, palladium and gold electrodes in 1 M sulfuric acid by cyclic voltammetry, *J. Electroanal. Chem.* 35 (1972) 209–218.

42. M.A. Montero, M.R.G. de Chialvo, A.C. Chialvo, Effects of the electrochemically grown hydrous oxide on the hydrogen electrode reaction on iridium electrode, *J. Electroanal. Chem.* 783 (2016) 106–111.

43. T. Wakelin, M. Smiljanić, Z. Rakočević, S. Štrbac, Catalysis of methanol oxidation on bimetallic Ir/Pt(poly) electrodes, *J. Nanosci. Nanotechnol.* accepted (2019).

44. E.N. El Sawy, V.I. Birss, Nanoengineered $Ir_{core}@Pt_{shell}$ nanoparticles with controlled Pt shell coverages for direct methanol electro-oxidation, *ACS Appl. Mater. Interfaces* 10 (2018) 3459–3469.

45. L.K. Ono, B. Yuan, H. Heinrich, B. Roldan Cuenya, Formation and thermal stability of platinum oxides on size-selected platinum nanoparticles: Support effects, *J. Phys. Chem. C* 114 (2010) 22119–22133.

46. D-H Lim, W-J Lee, N. L. Macy, W.H. Smyrl, Electrochemical durability investigation of PtÕTiO_2 nanotube catalysts for polymer electrolyte membrane fuel cells, *Electrochem. Solid-State Lett.* 12 (2009) B123–B125.

47. S.J. Freaklay, J. Ruiz-Esquius, D.J. Morgan, The X-ray photoelectron spectra of Ir, IrO_2 and $IrCl_3$, revisited, *Surf. Interface Anal.* 49 (2017) 794–799.

48. S. Kato, J. Jung, T. Suenobu, S. Fukuzumi, Production of hydrogen peroxide as a sustainable solar fuel from water and dioxygen, *Energy Environ. Sci.* 6, (2013) 3756–3764.

49. A.G. Wren, R.W. Phillips, L.U. Tolentino, Surface reactions of chlorine molecules and atoms with water and sulfuric acid at low temperatures, *J. Colloid Interface Sci.* 70 (1979) 544–557.

50. B.D. El-Issa, A. Katrib, R. Ghodsian, B.A. Salsa, S.H. Addassi, A comparative study of the bonding in different halides of iridium, *Int. J. Quantum Chem.* 33 (1988) 195–216.

51. P.G. Blake, A.F. Carley, V. Di Castro, M.W. Roberts, Chemisorptive replacement of surface oxygen by hydrogen halides (HCl and HBr) at Pb(110) surfaces. Photoelectron spectroscopic and kinetic evidence for a metastable chloride overlayer, *J. Chem. Soc. Faraday Trans. I* 82 (1986) 723–737.

52. S. Štrbac, M. Smiljanić, Z. Rakočević, Spontaneously deposited Rh on Au(111) observed by AFM and XPS: electrocatalysis of hydrogen evolution, *J. Electrochem. Soc*. 163 (2016) D3027–D3033.

53. S.J. Xia, V.I. Birss, In situ mass and ellipsometric study of hydrous oxide film growth on Pt in alkaline solutions, *Electrochim. Acta* 45 (2000) 3659–3673.

54. M.A. Montero, M.R.G. De Chialvo, A.C. Chialvo, Evaluation of the kinetic parameters of the hydrogen oxidation reaction on nanostructured iridium electrodes in alkaline solution *J. Electroanal. Chem.* 767 (2016) 153–159.

55. M.M. Jakšić, B. Johansen, R. Tunold, Electrochemical behavior of Iridium in alkaline and acidic solutions of heavy and regular water, *Int. J. Hydrogen Energy* 19 (1994) 321–335.

56. M. Łukaszewski, M. Soszko, A. Czerwiński, Electrochemical methods of real surface area determination of noble metal electrodes – an overview, *Int. J. Electrochem. Sci.* 11 (2016) 4442–4469.

57. S. Marini, P. Salvi, P. Neli, R. Pesenti, M. Villa, P. Berrettoni, G. Zangari, Y. Kiros, Advanced alkaline water electrolysis, *Electrochim. Acta* 82 (2012) 384–391.

58. B.E. Conway, B.V. Tilak, Interfacial processes involving electrocatalytic evolution and oxidation of H_2, and the role of chemisorbed H, *Electrochim. Acta* 47 (2002) 3571–3594.

59. N.M. Marković, S.T. Sarraf, H.A. Gasteiger, P.N. Ross, Hydrogen electrochemistry on platinum low-index single-crystal surfaces in alkaline solution, *J. Chem. Soc. Farraday Trans.* 92 (1996) 3719–3725.

60. B.E. Conway, L. Bai, Determination of adsorption of OPD H species in the cathodic hydrogen evolution reaction at Pt in relation to electrocatalysis, *J. Electroanal. Chem.* 198 (1986) 149–175.

61. B.V. Tilak, C.P. Chen, Generalized analytical expressions for Tafel slope, reaction order and a.c. impedance for the hydrogen evolution reaction (HER): mechanism of HER on platinum in alkaline media, *J. Applied. Electrochem.* 23 (1993) 631–640.

62. W. Sheng, H.A. Gasteiger, Y. Shao-Horn, Hydrogen oxidation and evolution reaction kinetics on platinum: Acid vs alkaline electrolytes, *J. Electrochem. Soc.* 157 (2010) B1529-B1536.

63. E. Skulason, G.S. Karlberg, J. Rossmeisl, T. Bligaard, J. Greeley, H. Jonsson, J.K. Norskov, Density functional theory calculations for the hydrogen evolution reaction in an electrochemical double layer on the Pt(111) electrode, *Phys. Chem. Chem. Phys.* 9 (2007) 3241-3250.

Figure captions

Figure 1. (a) OCP changes during immersion of Pt(poly) and Ir(poly) into neat 0.05 M H_2SO_4 and during spontaneous deposition of Ir onto Pt(poly) from 1mM $IrCl_3 \cdot xH_2O$+0.05 M H_2SO_4; (b) CVs of the Pt(poly), Ir(poly) and the obtained 30 min Ir/Pt(poly) electrodes recorded in neat 0.05 M H_2SO_4 solution at a scan rate of 50 mV s^{-1}.

Figure 2. AFM image (500 × 500) nm^2 of a bare Pt(poly) electrode surface showing: a) the topography (z–range 13.2 nm); b) cross section along the line indicated in the image.

Figure 3. AFM images (500 × 500) nm^2 of a Ir/Pt(poly) electrode obtained after 30 minutes deposition showing: a) surface topography (z–range 2.8 nm); b) cross section along the line presented in the height image; c) the corresponding phase image (z–range 11.5°); d) cross section along the line indicated in the phase image, the dashed line -3.0° separates a response from the deposited Ir islands and Pt(poly) surface; e) and f) resulting AFM image and cross section obtained after removing contributions from the Pt(poly) substrate.

Figure 4. FESEM-EDS characterization of bi-metallic Ir/Pt(poly) electrode: a) FESEM image; (b-d) corresponding EDS elemental mapping of O, Ir and Pt, respectively and e) EDS spectrum of the sample.

Figure 5. High resolution XPS spectra showing Pt 4f photoelectron lines taken from: a) Pt(poly); b) Ir/Pt(poly).

Figure 6. High resolution region XPS spectra taken from Ir/Pt(poly) showing the fitted binding energies of: a) Ir 4f; b) O 1s; c) Cl 2p photoelectron lines.

Figure 7. Cyclic voltamogramms of Pt(poly), Ir(poly) and Ir/Pt(poly) electrodes recorded in 0.1 M NaOH at a scan rate of 50 mV s^{-1}. Current densities are given with respect to EASAs.

Figure 8. Polarization curves for HER on Pt(poly), Ir(poly) and Ir/Pt(poly) electrodes recorded in hydrogen saturated 0.1 M NaOH at a scan rate of 10 mV s^{-1}. Current densities are given with respect to EASAs.

Figure 9. Tafel plots for HER on Pt(poly), Ir(poly) and 1 min Ir/Pt(poly) electrodes in 0.1 M NaOH obtained from steady-state measurements in hydrogen saturated 0.1 M NaOH at 1600 rpm. Inset shows a representative set of steady-state curves for HER recorded at η = 50 mV. From such curves recorded for different overpotentials, the data for current densities at t=200 s were taken for the construction of Tafel plots.

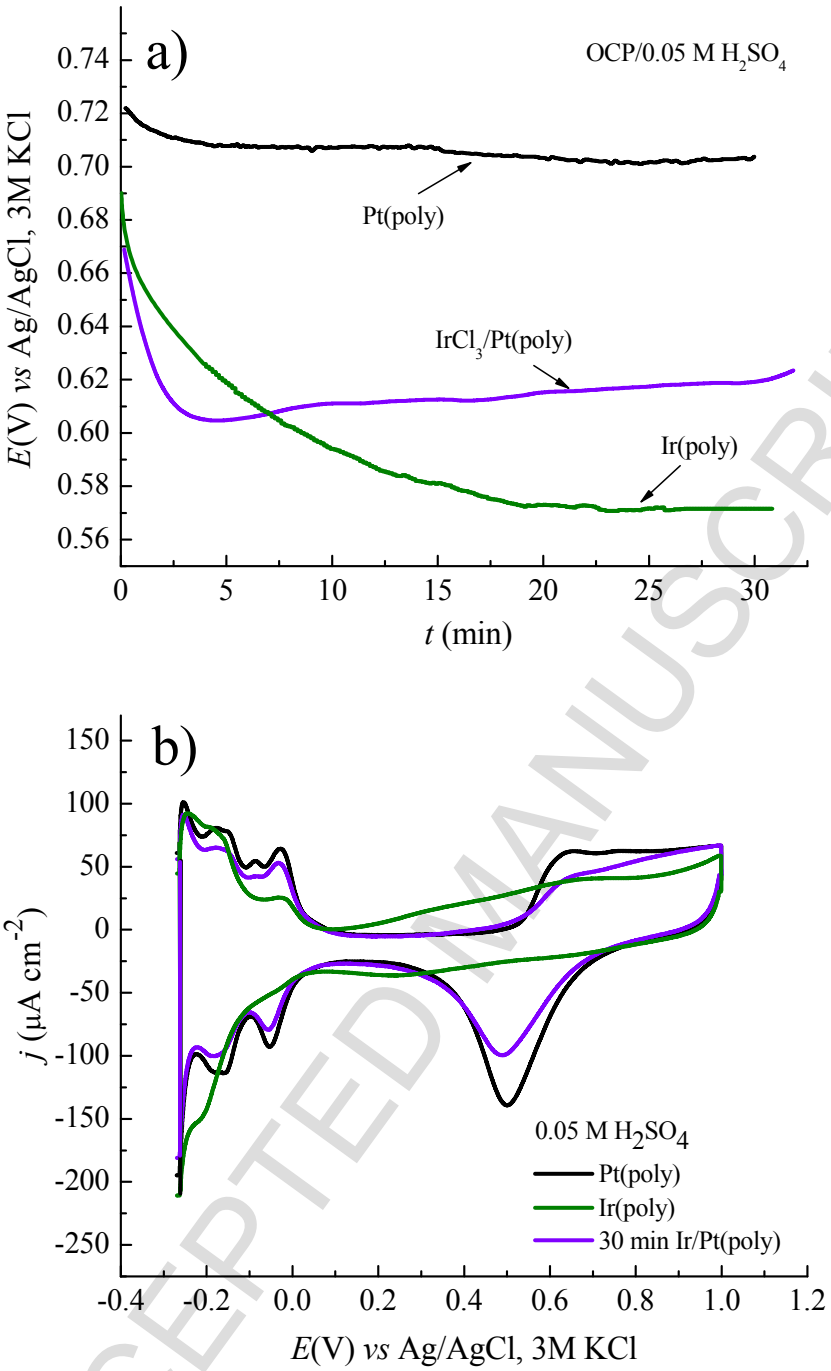

Figure 1

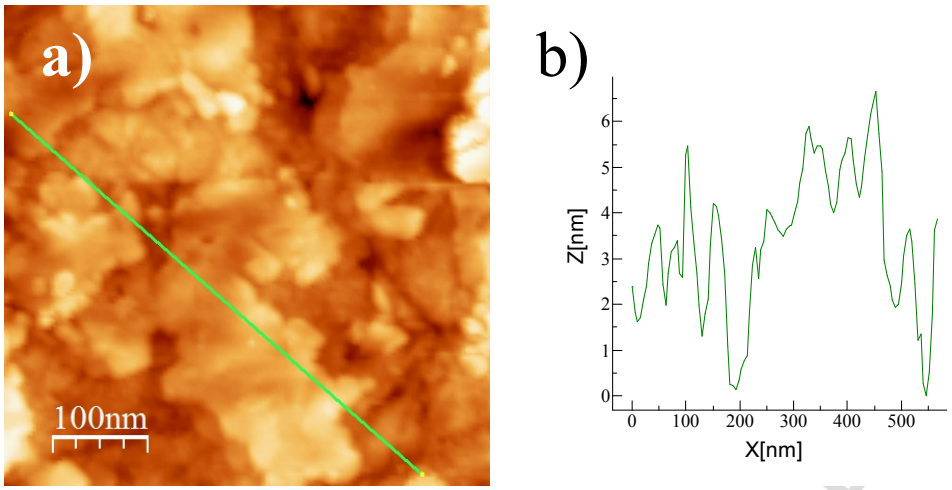

Figure 2

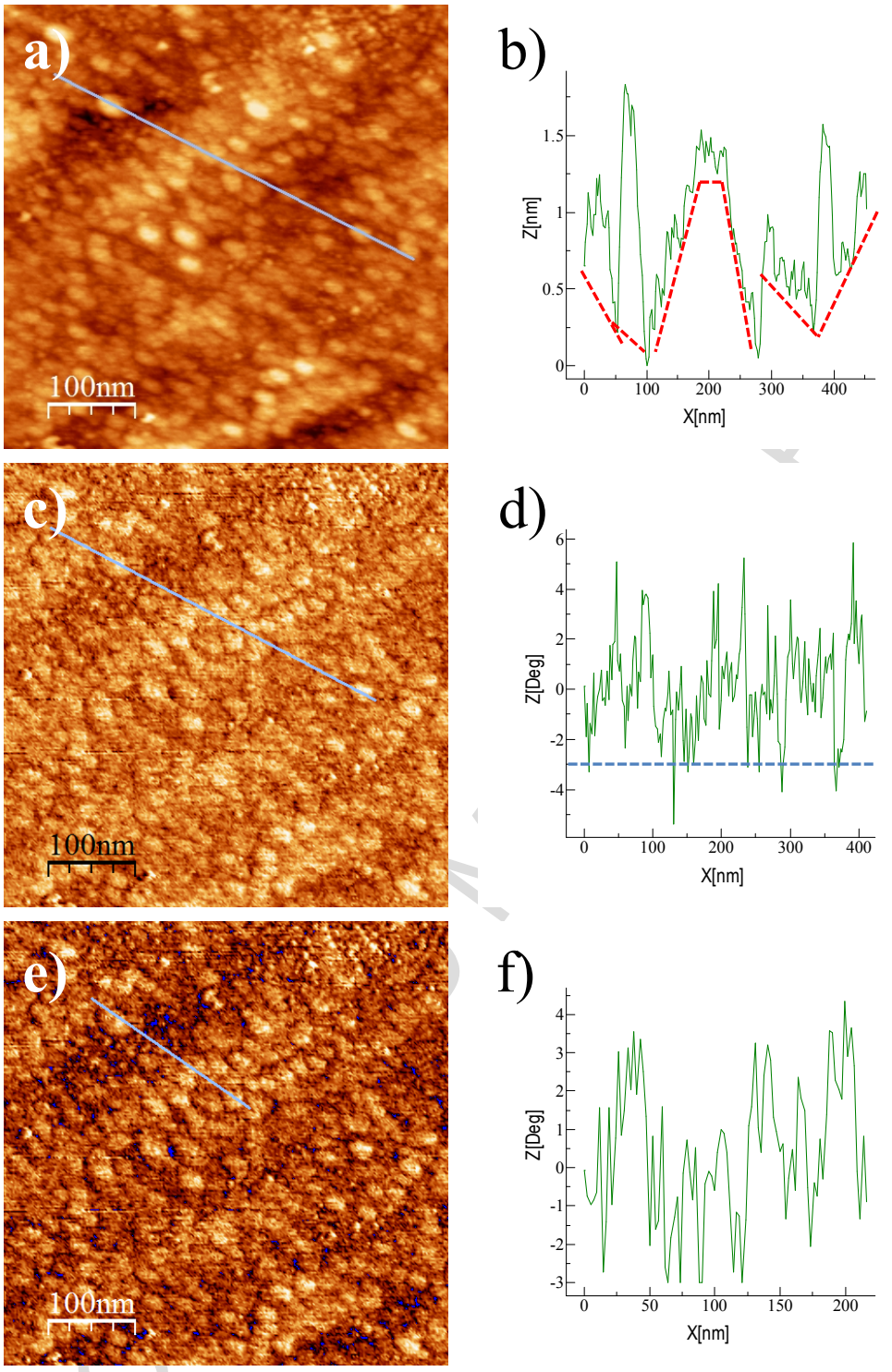

Figure 3

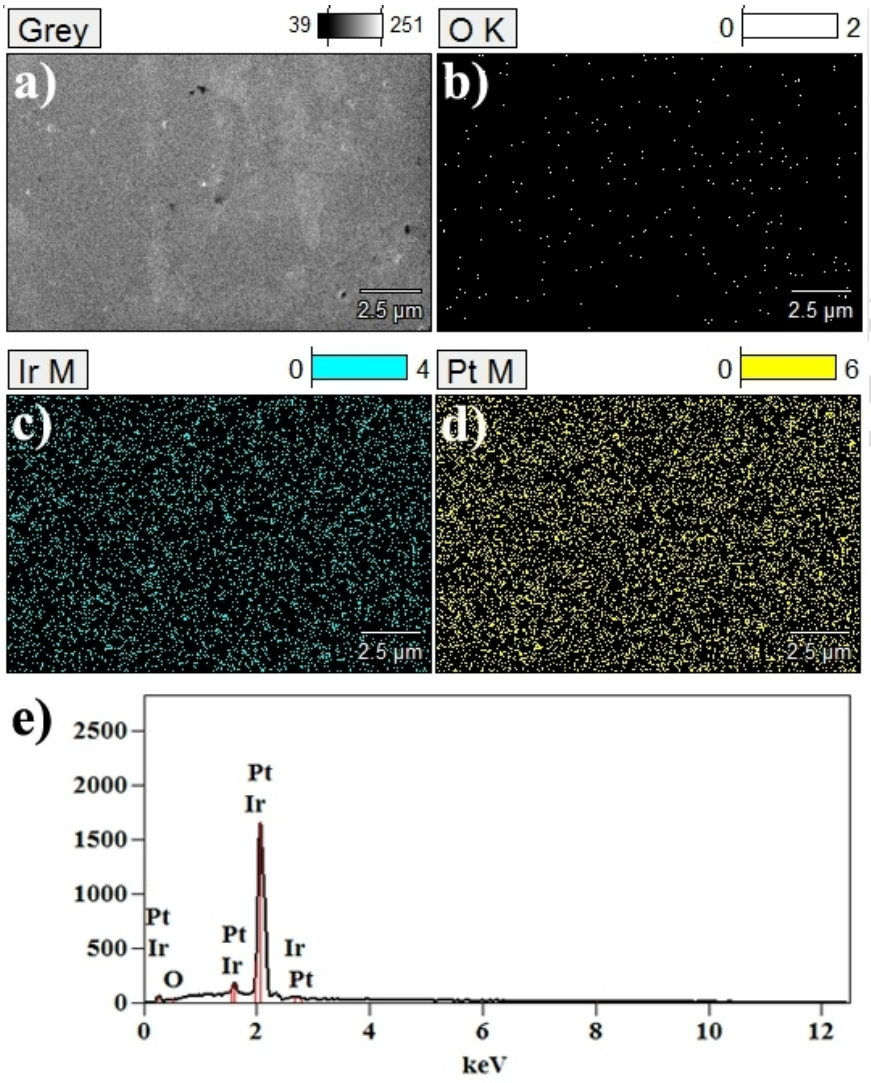

Figure 4

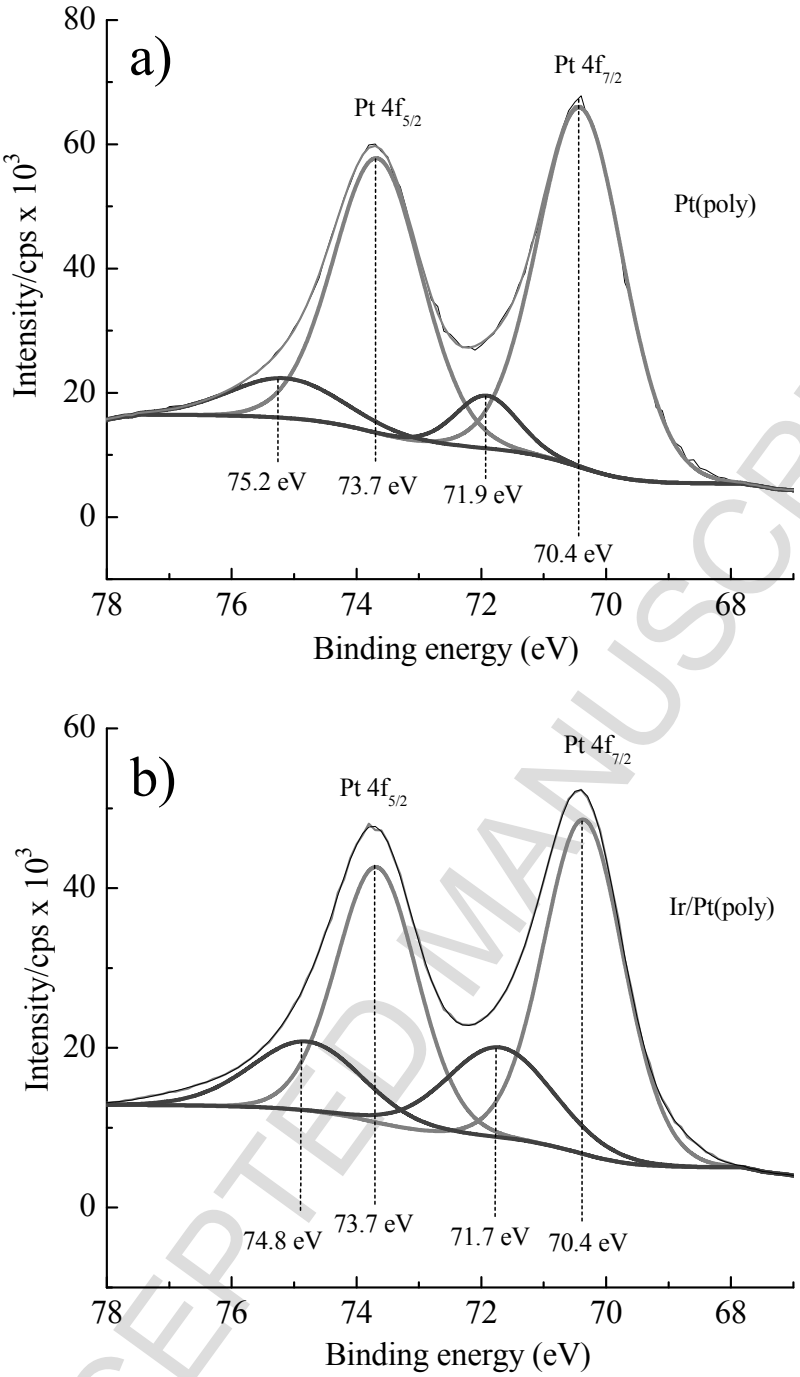

Figure 5

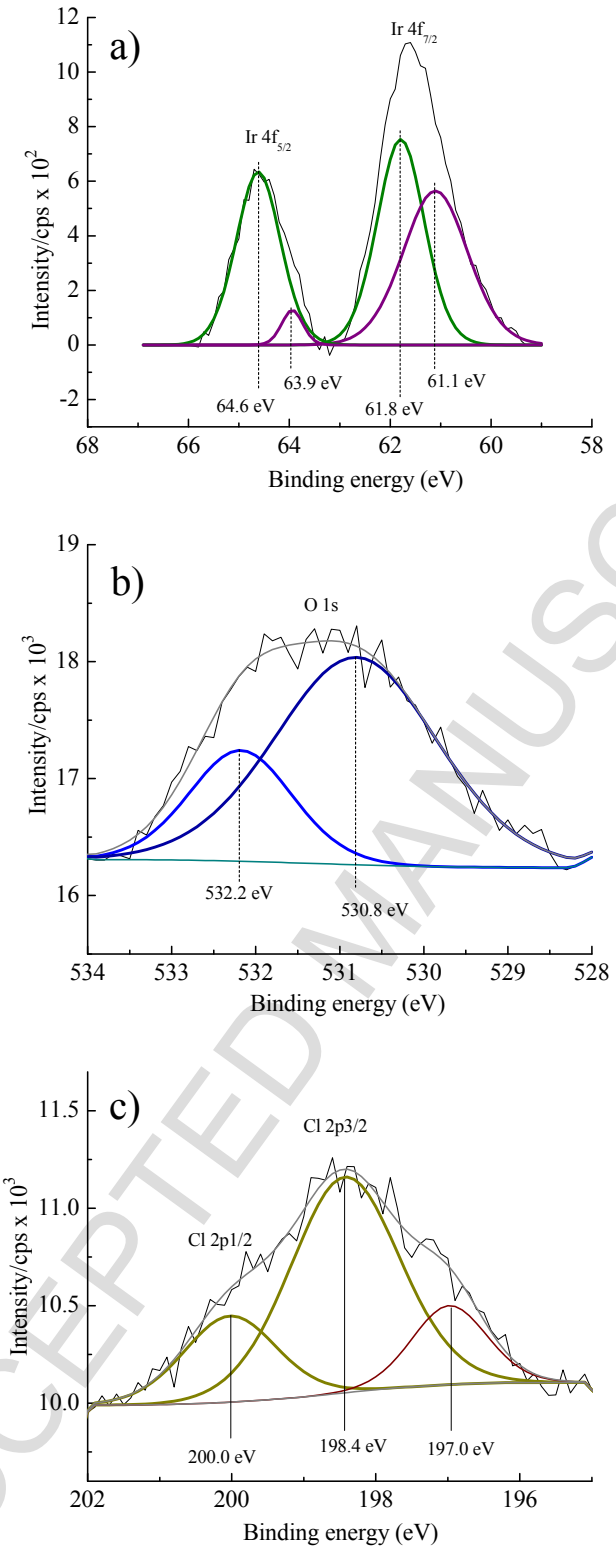

Figure 6

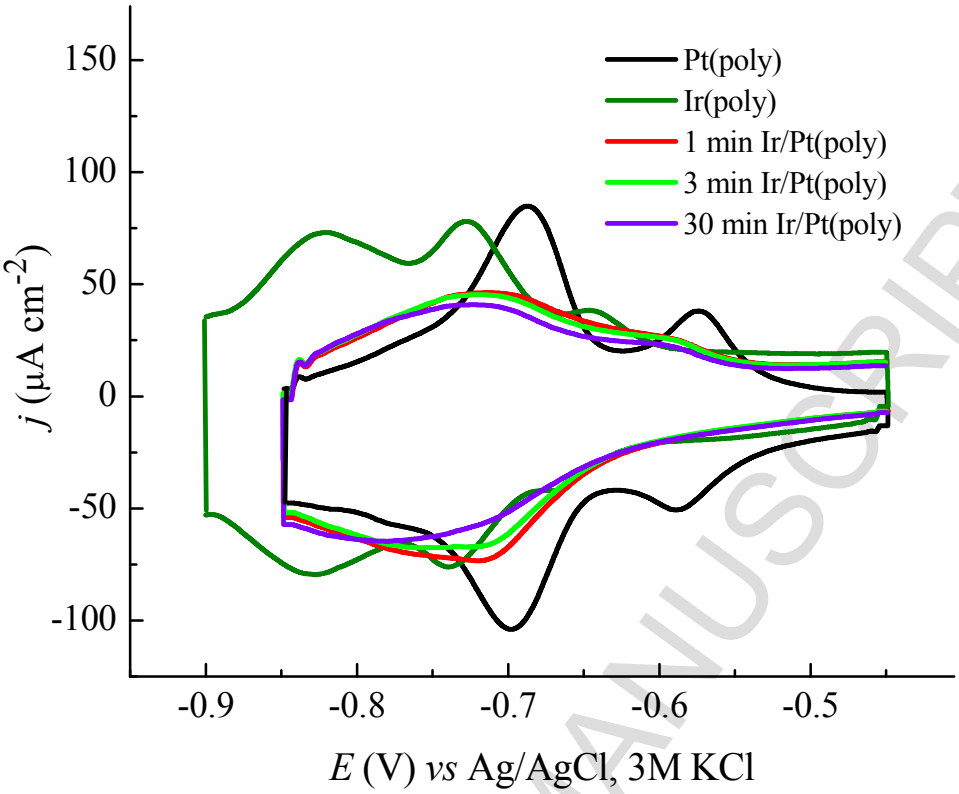

Figure 7

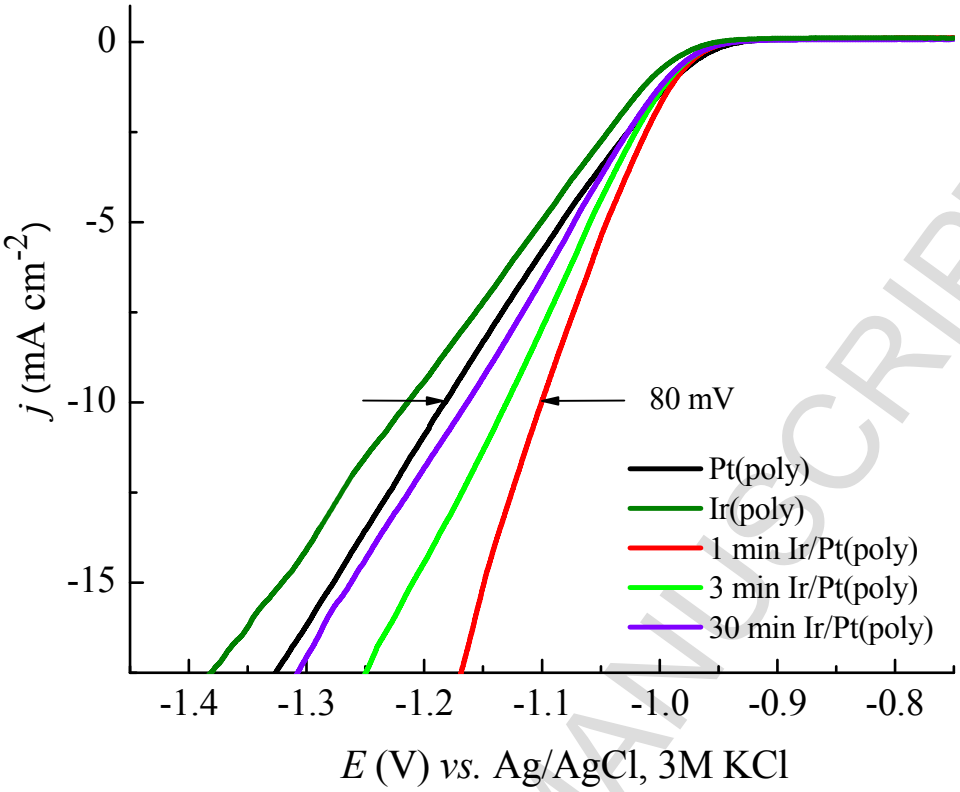

Figure 8

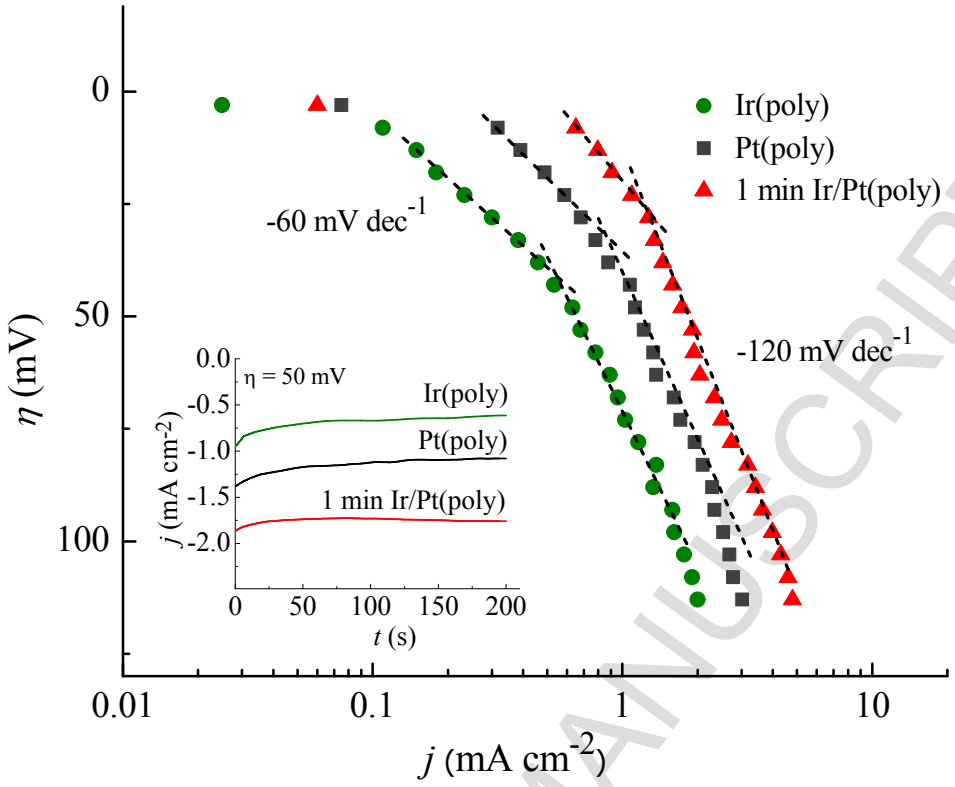

Figure 9

Highlights

- Bimetallic Ir/Pt(poly) electrodes were prepared by spontaneous deposition.
- Ir/Pt(poly) electrodes were characterized by AFM, FESEM and XPS.
- The highest activity for HER in alkaline solution was obtained on 80% Ir/Pt(poly).
- Enhanced HER activity was ascribed to the synergistic effect.